ChemPubSoc Europe
DOI: 10.1002/cssc.201500845
CHEMSUSCHEM Full Papers

All-Iron Redox Flow Battery Tailored for Off-Grid Portable Applications

Michael C. Tucker,* Adam Phillips, and Adam Z. Weber[a]

An all-iron redox flow battery is proposed and developed for end users without access to an electricity grid. The concept is a low-cost battery which the user assembles, discharges, and then disposes of the active materials. The design goals are: (1) minimize upfront cost, (2) maximize discharge energy, and (3) utilize non-toxic and environmentally benign materials. These are different goals than typically considered for electrochemical battery technology, which provides the opportunity for a novel solution. The selected materials are: low-carbon-steel negative electrode, paper separator, porous-carbon-paper positive electrode, and electrolyte solution containing 0.5 M $Fe_2(SO_4)_3$ active material and 1.2 M NaCl supporting electrolyte. With these materials, an average power density around 20 mW cm^{-2} and a maximum energy density of 11.5 Wh L^{-1} are achieved. A simple cost model indicates the consumable materials cost US$6.45 per kWh^{-1}, or only US$0.034 per mobile phone charge.

Introduction

Access to energy is critically lacking throughout the developing world.[1] Purchasing electricity for basic household needs such as LED lighting, mobile phone charging, and radio is expensive and difficult. Solar home systems are beyond the means of most of these households, and charging mobile phones at pay-per-charge kiosk businesses is time consuming and expensive, costing about US$0.25 per charge. Kerosene lighting is also expensive, with fuel costs around US$4 per month for a household.[2]

The present work assesses the technical and economic feasibility of an extremely inexpensive, long shelf-life, nontoxic battery concept proposed to enable access to electricity for typical bottom-of-the-pyramid consumers. These consumers are extremely price conscious, have a real unmet need, and do not generally have access to waste-stream recycling. Spent batteries are expected to be disposed of in the normal household waste stream. In many areas, this means spent material will be dumped outside the dwelling or into open-pit sewers, making selection of environmentally benign materials just as important as human health considerations.

To address these opportunities and constraints, we propose a low-cost, chemically rechargeable battery composed of materials that are benign. The goal is an intuitive and affordable product that allows users to generate a small amount of electricity on-demand, in their own home (e.g., for LED lighting or mobile phone charging). The user will insert active materials into the cell periodically, before every discharge, and spent material is simply disposed. The cell is "recharged" by replacing the active materials as opposed to electrochemical charging through an external electricity supply. This frees the designer to optimize discharge performance, with no need to address electrochemical charge performance. Further benefits expected of this design include a long shelf life, as active materials are not in contact with each other until the time of use, and reduced delivery costs, as there is no water or other solvent weight to be transported from the manufacturing facility to the end user.

The product concept includes a durable cell housing that accepts the consumable cell materials, including anode, cathode, and separator, and when closed holds them in compressed contact. The end user would do as much assembly as is practical to minimize up-front cost. The housing also has electrical contacts for the anode and cathode and ports for the catholyte to enter and exit. The user is responsible for mixing the catholyte salt, provided as a packet or tablet, with locally available water and pouring it into the cathode vessel. The exiting solution can be collected and passed through the cell again to increase total utilization of the chemicals. The cell is comprised of inexpensive materials, and many of the materials are replaced at regular intervals, some before every discharge, to relieve the constraint of long-term stability and cycle life.

The design goals for this application are: (1) minimize up-front cost, (2) maximize discharge energy with respect to the cost of consumable materials, and (3) limit the choice of materials to those that are non-toxic and environmentally benign. This is a different set of goals than typically considered for electrochemical battery technologies and provides the opportunity for a novel optimization solution.

To meet the above targets, an all-iron system that uses iron metal and ferric ions is attractive. Iron, among the common metals, is notable for its low cost, low health risk, and ubiquitous availability. The all-iron redox flow cell was introduced more than 30 years ago,[3] and several groups have made prog-

[a] Dr. M. C. Tucker, A. Phillips, Dr. A. Z. Weber
Energy Storage and Distributed Resources Division
Lawrence Berkeley National Laboratory
1 Cyclotron Rd. MS70-108b, Berkeley, CA 94720 (USA)
E-mail: mctucker@lbl.gov

ress by improving efficiency via decreased hydrogen generation during charging;[4–6] increasing iron plating density and efficiency;[7] preventing precipitation of iron salts through complexation;[8] and manipulating the redox window through modification of the iron ligand present in solution.[8] Many of the issues that are the focus of previous all-iron flow battery research are not a concern for the present concept because electrochemical charging does not occur. In essence, the present work is a reoptimization of the all-iron redox flow cell given a new set of goals and constraints set by the developing world product concept.

The critical electrochemical cell components are shown schematically in Figure 1, with the reactions:

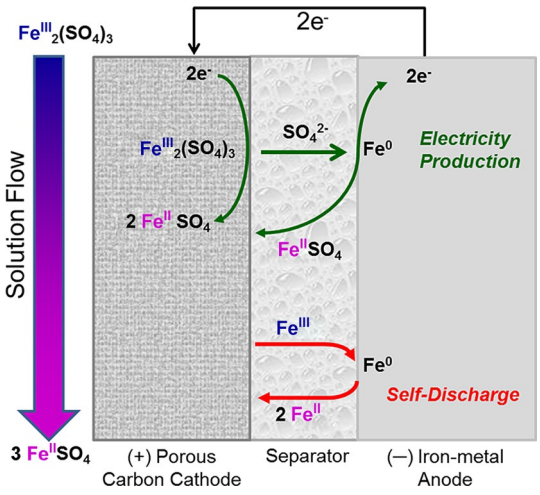

Figure 1. Schematic of cell during discharge. The desired electricity-producing reactions and undesired self-discharge (iron disproportionation) reactions are indicated.

$$\text{Cathode} \quad 2\,Fe^{3+} + 2\,e^- \rightarrow 2\,Fe^{2+} \quad E^0 = 0.77\ \text{V vs. SHE} \quad (1)$$

$$\text{Anode} \quad Fe^0 \rightarrow Fe^{2+} + 2\,e^- \quad E^0 = -0.44\ \text{V vs. SHE} \quad (2)$$

$$\text{Total} \quad 2\,Fe^{3+} + Fe^0 \rightarrow 3\,Fe^{2+} \quad E^0 = 1.21\ \text{V} \quad (3)$$

The anode is iron metal, and the cathode is a carbon porous electrode (CPE). They are prevented from electronic short circuiting by a separator that allows ion transfer between the electrodes. The active cathode material is Fe^{3+}, which is present as an aqueous salt that flows through the CPE and which reacts on its surfaceReactions (1) and (2) are the desired electrochemical reactions during discharge and are accompanied by sulfate transport through the separator. Reaction (3) is the total desired reaction, a sum of Reactions (1) and (2). This reaction may also occur, however, by chemical comproportionation of Fe^{3+} in contact with Fe^0 arising from crossover of Fe^{3+} through the membrane to the surface of the iron metal electrode. Essentially, crossover Fe^{3+} etches the metallic iron electrode rather than contributing to the desired electrochemical reaction. Thus, Fe^{3+} crossover through the membrane introduces self-discharge inefficiency and should be minimized.

Results and Discussion

Iron solution characterization

Solutions of $Fe_2(SO_4)_3$ and $FeCl_3$ were prepared in the concentration range 0.25 to 2 M. Conductivity, pH value, and viscosity of these solutions is shown in Figure 2. As is typical for simple

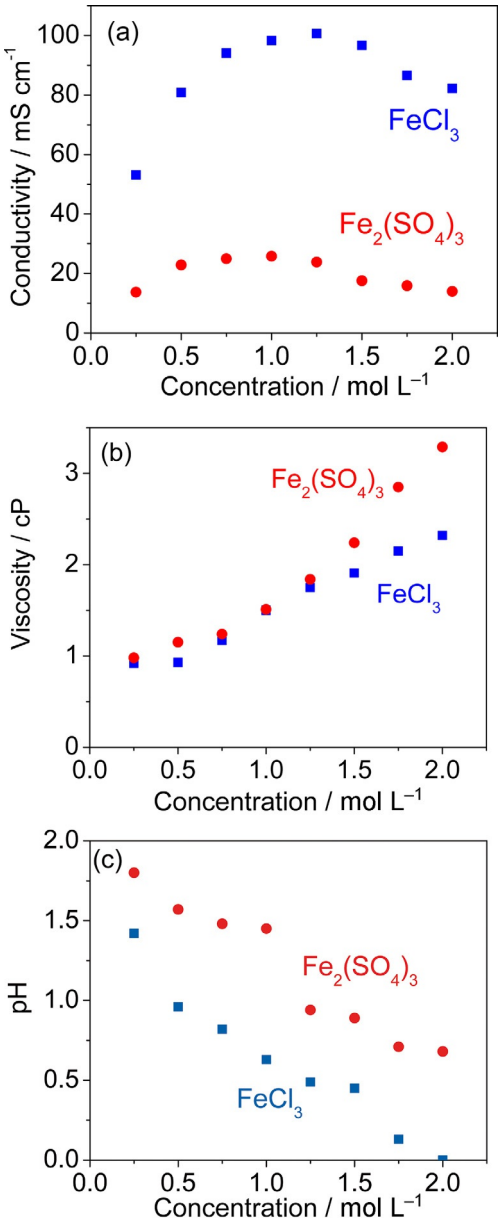

Figure 2. Dependence of (a) conductivity, (b) viscosity, and (c) pH value on the concentration of aqueous $Fe_2(SO_4)_3$ (circles) and $FeCl_3$ (squares).

salt solutions, conductivity initially increases with molarity due to increasing concentration of charge carriers, then peaks and decreases due to increased solution viscosity and, therefore, reduced ion mobility. Conductivity of the sulfate solutions is significantly lower than for chloride solutions, and this was the basis for selecting the iron chloride system as the focus of

early work with the all-iron battery.[3] Viscosity increases roughly linearly in the concentration range studied, which is a concern for the simple system addressed here, as increased viscosity will increase the requirement for continuous mechanical pumping energy (delivered by hand) or tank and cell pressure if the system is pressurized only at the beginning of the discharge run. If the solution is gravity fed, high viscosity will reduce the flowrate through the (+) CPE. Upon discharge, solution concentration increases as iron is stripped from the (−) metal electrode due to Reaction 2. For example, 0.5 M $Fe_2(SO_4)_3$ (23 mS cm^{-1} conductivity, 1.2 cP viscosity, and pH 1.6) will discharge completely to 1.5 M $FeSO_4$ (66 mS cm^{-1} conductivity, 2.8 cP viscosity, and pH 2.8). Thus, discharge causes a moderate increase in conductivity, viscosity, and pH value.

The native pH value of these solutions is quite low. Fortuitously, the operating pH window is well below pH 3.5. Above that value, the iron salts convert to iron hydroxide, a low-solubility salt that tends to precipitate out of solution. During electrochemical charging of the conventional all-iron battery, the pH value can rise above this limit, and buffering, addition of ligands, or other measures must be taken to avoid precipitation.[8] The design choice of limiting the present system to only discharge eliminates this complication.

In the rechargeable all-iron cell, the typical iron salt is $FeCl_3$, chosen for its high solubility and conductivity in aqueous solution.[3,8] In this work, we must also account for the potential for negative human and environmental health impacts. Iron sulfate is a source of iron used in dietary supplements and is used in dentistry and wastewater cleanup. In contrast, $FeCl_3$ is a chemical etchant and suspected to be harmful to aquatic life. The cost for each is less than US$300 per ton. Based on these considerations, the focus of this work is determining and improving performance using the more benign iron sulfate. We do, however, include some results with iron chloride for comparison.

Separator screening and selection

A wide range of commercially available anion exchange membranes (AEM), proton exchange membranes (PEM), microporous separators, and papers were screened for open-circuit voltage (OCV) and initial performance. Most candidates were removed from further consideration due to low OCV or poor initial discharge performance. Polarization is shown for the three remaining candidates with both 0.5 M $Fe_2(SO_4)_3$ and 1 M $FeCl_3$ in Figure 3. The different salt molarities are chosen to make a comparison between solutions with the same Fe^{3+} ion concentration. The anion exchange membrane (Ameridia AMX) shows the highest OCV [close to that predicted by Eq. (3)], whereas the others have an OCV significantly below the theoretical value. This is probably due to high crossover, which causes self-discharge and concomitant deviation from the standard potential at the iron metal anode as shown in Figure 1. The flux of Fe^{2+} back to the cathode may also reduce the potential due to Nernstian effects. Despite the high OCV for AMX, the slope of the polarization curve, which is indicative of the area-specific resistance (ASR) limits the peak power. Paper also

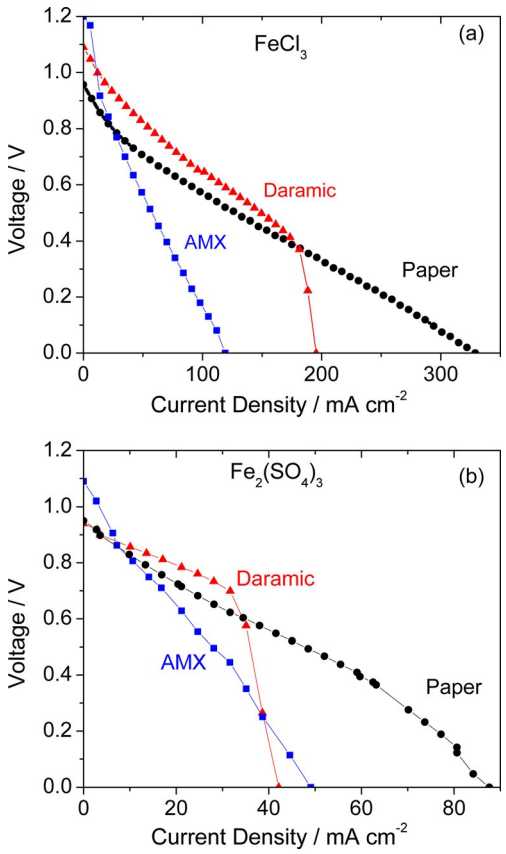

Figure 3. Effect of membrane on performance with (a) 1 M $FeCl_3$ or (b) 0.5 M $Fe_2(SO_4)_3$. Membrane types: AMX (squares), Daramic (triangles), printer paper (circles).

displays a roughly linear polarization curve, but has significantly lower resistance. In contrast, Daramic shows limiting-current behavior, which limits peak power in the case of $Fe_2(SO_4)_3$. We surmise the limiting current arises from mass transport limitation in the membrane as the high current density achieved for paper indicates mass transport in the (+) electrode is sufficient. Note that the Daramic membrane is roughly three times thicker than the paper compared in Figure 3. The limiting current for $Fe_2(SO_4)_3$ is significantly lower than for $FeCl_3$. This comparison highlights that the design goal of eliminating health and environmental risk also means accepting the lower performance of the sulfate salt.

Peak power density is shown for paper, AMX, and Daramic membranes as a function of $Fe_2(SO_4)_3$ concentration in Figure 4. The peak power generally decreases with increasing concentration due to the viscosity and conductivity trends shown in Figure 3. Note that AMX is significantly more expensive than Daramic and paper and provides no performance benefit. It was, therefore, eliminated from further consideration.

Various types of office paper were tested, including different colors, thicknesses, and surface finishes. One clear trend is that performance depends on paper thickness, as shown in Figure 5. All papers provided relatively linear discharge polarization curves, but thicker paper produced much higher area-specific resistance (ASR). Peak power density and ohmic impe-

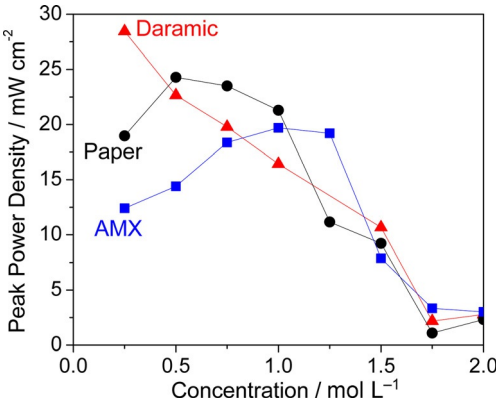

Figure 4. Effect of $Fe_2(SO_4)_3$ concentration on performance. Membrane types: AMX (squares), Daramic (triangles), office paper (circles).

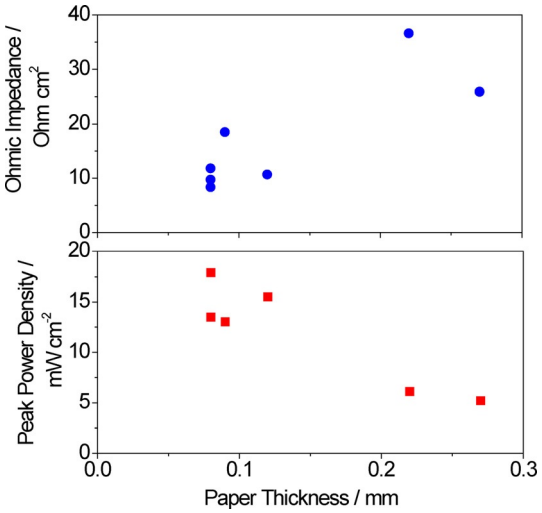

Figure 5. Effect of paper separator thickness on power density (squares) and ohmic impedance (circles) with 0.25 M $Fe_2(SO_4)_3$.

dance are correlated to paper thickness in Figure 5, and the results are consistent with ohmic loss in the membrane dominating cell performance for the case of paper. There is some scatter in the correlation, suggesting a secondary influence in addition to thickness. We did note that solution conductivity increased after wetting the paper in the solution, and the magnitude of this effect varied significantly between the various paper types. Presumably this arises from paper-making additives dissolving or affecting solution pH values. We did not study this phenomenon systematically as the intentional addition of supporting electrolyte had a much larger impact on cell performance as discussed in the following section.

Supporting electrolyte

The impact of paper thickness and the observation of higher performance for $FeCl_3$, which has a much higher conductivity than $Fe_2(SO_4)_3$, suggests that ohmic losses in the solution phase dominate cell performance. We, therefore, increased solution conductivity through addition of supporting electrolyte salts, as shown in Figure 6a. This also increases the limiting

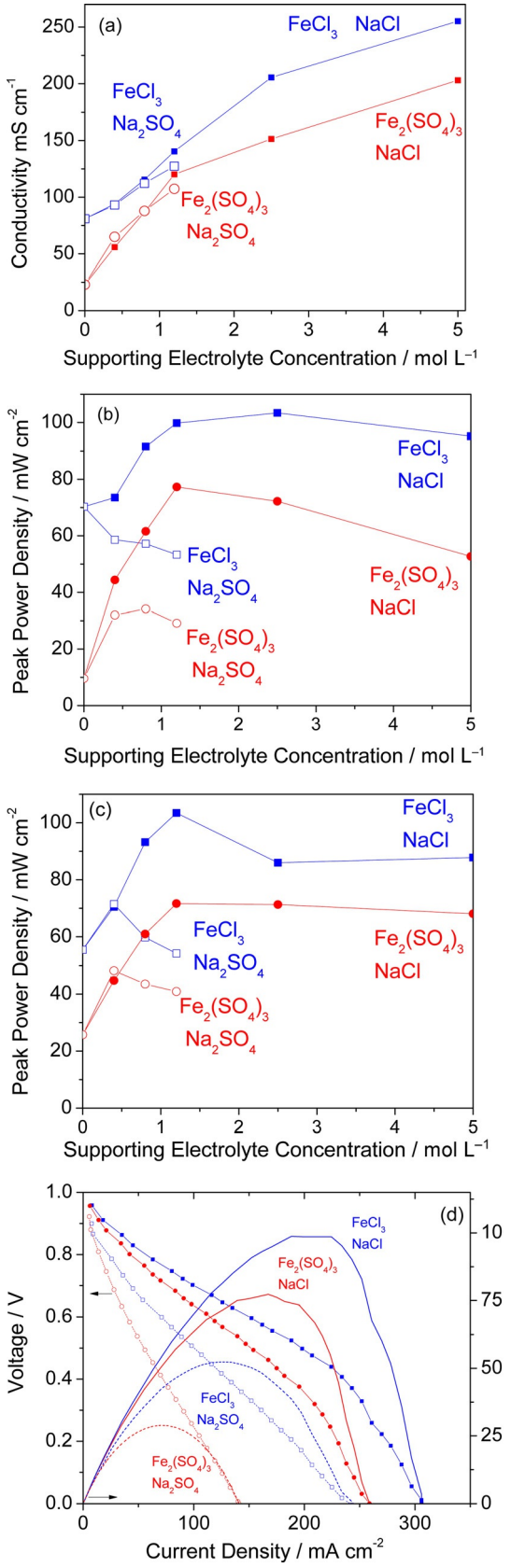

Figure 6. Effect of supporting electrolyte concentration on properties for solutions with 0.5 M $Fe_2(SO_4)_3$ (circles) and 0.5 M $FeCl_3$ (squares) with additional supporting electrolyte salt: NaCl (closed symbols) or Na_2SO_4 (open symbols): (a) Solution conductivity, peak power using (b) paper and (c) Daramic as separator, and (d) performance using paper as separator and 1.2 M supporting electrolyte salt.

current as the supporting electrolyte introduces charge carriers that are not involved in the reactions and, therefore, are not diffusion limited across the separator at the low limiting currents observed in Figure 3. Na_2SO_4 and NaCl were chosen because they are easily soluble, inexpensive, and benign. The rate of increase of solution conductivity with increasing supporting electrolyte concentration is similar for both salts, and the solutions with $FeCl_3$ remain consistently higher than with $Fe_2(SO_4)_3$. Note that higher concentrations of NaCl are achievable due to the solubility limits of 6.1 M for NaCl and 1.5 M for Na_2SO_4.

The impact of supporting-electrolyte concentration on peak power density for cells with paper and Daramic separators is shown in Figure 6b and c. The general trend is that increasing the supporting electrolyte salt concentration initially increases cell power due to increased conductivity. This is consistent with the ohmic impedance for 0.5 M $Fe_2(SO_4)_3$ solution and paper separator, which decreased from 15.3 Ohm cm^2 (with no supporting electrolyte) to 9.3 and 2.6 Ohm cm^2 for 1.2 M Na_2SO_4 and NaCl, respectively. The cell power peaks and declines at higher concentrations as mass-transport limitations begin to restrict peak power, presumably due to increased solution viscosity. Polarization curves are compared for 1.2 M addition of supporting electrolyte in Figure 6d. A maximum peak power of roughly 75 mW cm^{-2} is achieved for 0.5 M $Fe_2(SO_4)_3$ by addition of 1.2 M NaCl, which compares favorably to the power density in the range of 20–50 mW cm^{-2} reported previously for the all-iron battery.[3,9] This electrolyte formulation is used to characterize discharge behavior of the cell (see below). The impact on the toxicity and environmental hazard of adding NaCl to the solution at the point of use is unclear and should be addressed in the future. If NaCl is found to be undesirable, improved performance can still be expected when using Na_2SO_4 or another benign salt.

Electrode effects

Various types of (+) CPE and (−) iron metal electrode were tested to assess the impact of each electrode on cell performance and evaluate the potential of electrode optimization to increase cell performance. The effect of CPE type is show in Figure 7. The primary impact is on discharge polarization slope (ASR). The 10AA and H2315 performed significantly better than MRC U105.

Figure 8 compares discharge polarization curves for various (−) iron-metal electrode types. For the dense sheet types, commercial-grade gray cast iron (96% Fe) and low-carbon steel (98.5% Fe) were used because they are widely available and less expensive than high-purity iron and thus well suited to be used as a low-cost disposable electrode. The primary alloying elements for both types are C, Mn, and Si. Low-carbon steel provided the best performance, possibly due to the higher iron content or favorable kinetics arising from grain structure or other metallurgical properties. A 2 mm thick porous coupon of sintered pure iron particles provided similar polarization to dense cast iron, suggesting that surface area for iron oxidation (Reaction 2) does not limit performance. The impact of the

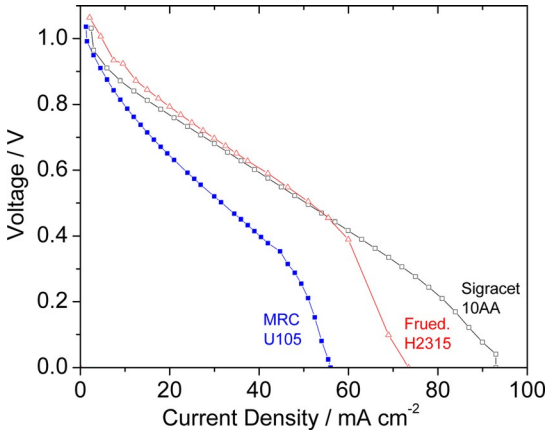

Figure 7. Comparison of various (+) CPE materials with Daramic separator and 0.5 M $Fe_2(SO_4)_3$ solution. Sigracet 10AA (open squares), Fruedenberg H2315 (Frued., open triangles), MRC U105 with PTFE loading of 0% (closed squares).

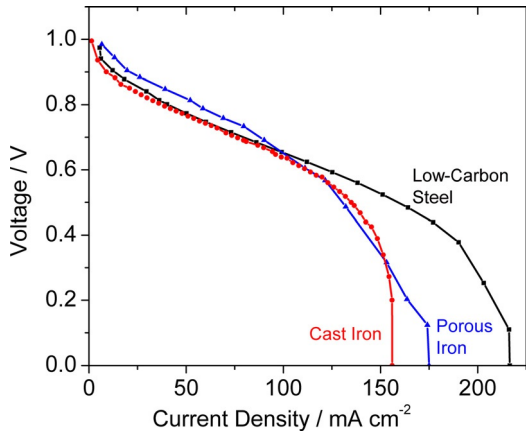

Figure 8. Comparison of various (−) iron-metal electrode types using paper as separator and 0.2 M $Fe_2(SO_4)_3$ + 3 M NaCl as electrolyte: Low-carbon-steel sheet (squares), gray cast iron sheet (circles), and sintered porous iron (triangles).

iron-metal electrode type was much smaller than the impact of (+) CPE discussed above. Low-carbon steel was selected for all experiments described below.

Discharge behavior

When the cell is discharged, Fe^{3+} at the (+) electrode and Fe^0 at the (−) electrode are both converted to Fe^{2+}, decreasing the Fe^{3+} concentration but increasing the total iron concentration in solution. This reduces the potential and leads to changes in solution properties. Upon complete discharge, a solution of 0.5 M $Fe_2(SO_4)_3$ with 1.2 M NaCl (60 mS cm^{-1} conductivity, 2.8 cP viscosity, and pH 1.8) changes to 0.75 M $FeSO_4$ with 1.2 M NaCl (63 mS cm^{-1}, 3.0 cP, pH 2.5). Furthermore, as the (−) electrode is consumed, cell compression and (+) electrode thickness may change and gaps may form at the separator/(−) electrode interface. For these reasons, cell performance is not expected to remain constant as the state of charge (SOC) de-

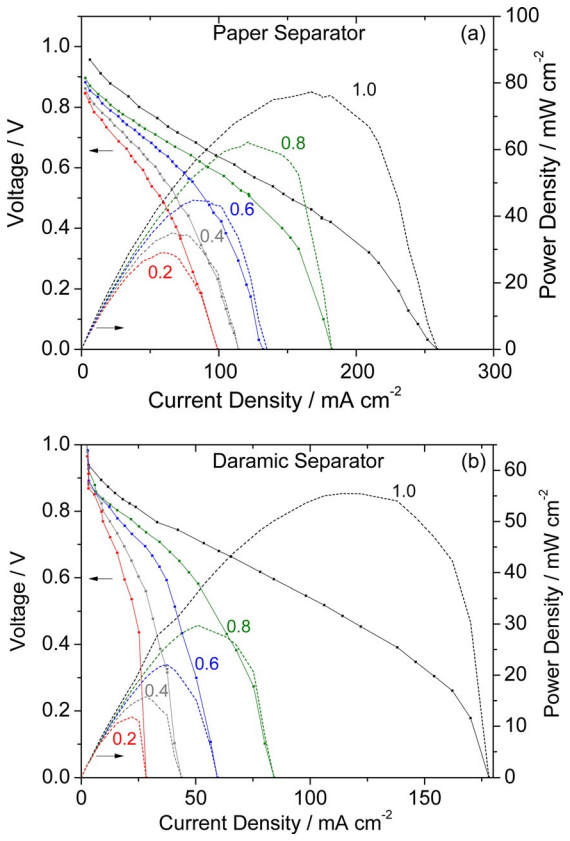

Figure 9. Effect of SOC on performance using (a) paper or (b) Daramic as separator. SOC is labeled in the Figure (fully charged = 1.0).

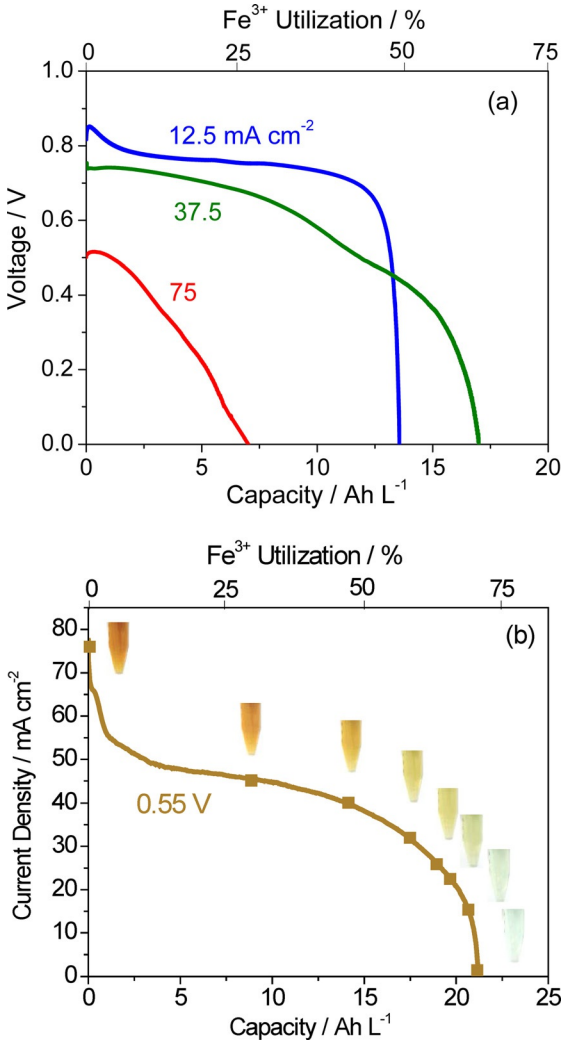

Figure 10. Discharge of 0.5 M $Fe_2(SO_4)_3$ + 1.2 M NaCl solution using paper as separator under conditions of: (a) constant current, with current density labeled in the graph; or (b) constant voltage (0.55 V; images of the solution at various points along the constant-voltage discharge curve are inset to show the color change).

creases during continuous discharge. Figure 9 shows how the performance evolves as a function of SOC. The OCV for paper as separator is always lower than for Daramic, likely arising from higher crossover of Fe^{3+} through the thinner paper. The ASR slope of the discharge curves increases as Fe^{3+} is consumed, presumably due to both decreased reactant concentration and increased solution viscosity. The overall result is that peak power declines dramatically as discharge proceeds. The paper separator produced higher power than Daramic at all SOC; thus, it was selected for use in the experiments discussed below.

Cells were discharged at various current densities and voltages to optimize the total energy extracted from the consumable materials. Note that excess iron metal was used at the (−) electrode; thus, theoretical capacity is limited by Fe^{3+}. Selected constant-current discharges are shown in Figure 10a. At high current density (75 mA cm^{-2}), polarization losses lead to low output voltage and curtail the capacity. At low current density (12.5 mA cm^{-2}), voltage remains high throughout the entire discharge and the sharp change of the curve at the end of discharge suggests complete consumption of Fe^{3+}. At such low operating currents, however, the self-discharge current becomes a significant source of inefficiency and consumes a large portion of the Fe^{3+}, leading to low utilization. We suspect self-discharge is reduced at low SOCs, where the concentration of Fe^{3+} is lower. At intermediate current density (37.5 mA cm^{-2}), the voltage remains relatively high and utilization is improved. A typical constant-voltage discharge is shown in Figure 10b. Initially, the current decreases rapidly, presumably due to both ASR and mass transport effects (see Figure 9a), but then remains between 30 and 50 mA cm^{-2} throughout most of the discharge period, and finally drops rapidly at the end of discharge. Again, Fe^{3+} utilization is less than 100% due to self-discharge. The images inset to Figure 10b show the color of the solution in the reservoir (a clear plastic vial). The color remains brown until about 90% of the capacity is utilized and then quickly changes to faint blue. This provides a clear visual indication to the end user that all Fe^{3+} in the solution is consumed and another batch of fresh solution is required to generate more energy. The surface of the iron metal is heavily pitted after discharge, although this does not prevent it from being reused during subsequent discharge runs until it is consumed. The iron is also wet after cell disassembly, suggesting that any gaps between the paper and

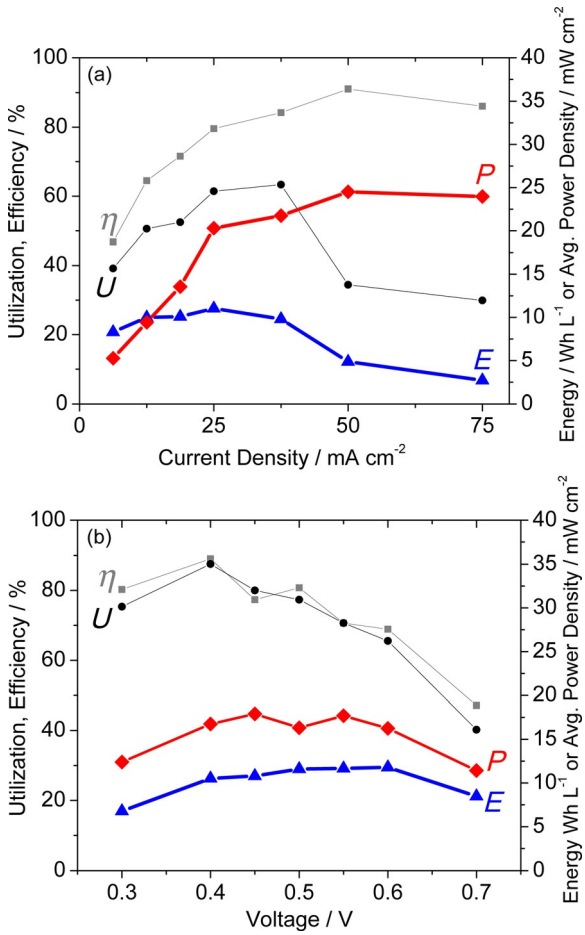

Figure 11. Performance metrics determined from (a) constant-current or (b) constant-voltage discharges such as those shown in Figure 10 with 0.5 M $Fe_2(SO_4)_3$ + 1.2 M NaCl solution and paper separator. Discharge energy (*E*, triangles), average power density (*P*, diamonds), coulombic efficiency (η, squares), and Fe^{3+} utilization (*U*, circles) are shown.

metal caused by pits are filled with electrolyte. Thus, the pitted area is expected to continue functioning, albeit with a slightly higher local ohmic resistance due to the longer ion path between the positive electrode and bottom of the pit.

Figure 11 summarizes the impact of current density or voltage selection on average power, discharge energy, coulombic efficiency, and utilization of the consumable $Fe_2(SO_4)_3$. For constant-current operation (Figure 11 a), the average power increases rapidly with current density up to 25 mA cm^{-2}, above which power is constrained by a low cell voltage (see Figure 10 a). At 50 mA cm^{-2} and higher, energy is impacted by underutilization of the Fe^{3+}, as described above. For constant-voltage operation (Figure 11 b), there is a broad maximum in power. Power drops as expected at very low voltage or current (which occurs at high voltage approaching the OCV). There is a broad maximum in energy for both constant-current and constant-voltage operation ranging from 12.5 to 37.5 mA cm^{-2} and 0.4 to 0.6 V. This makes the system forgiving of operating point variation and suggests that there is scope to implement more sophisticated control strategies, such as peak power tracking, to further optimize energy delivery.

Solution utilization refers to the fraction of Fe^{3+} used to produce power (as opposed to being consumed by self-discharge or remaining in solution after cell voltage reached the cutoff of 0 V in the case of constant current), and is taken as the ratio of discharge capacity to the theoretical solution capacity [26.8 Ah L^{-1} for 0.5 M $Fe_2(SO_4)_3$]. Utilization is reduced at high current density, at which the lower voltage limit is engaged before all of the Fe^{3+} is consumed (see Figure 10 a). This effect is not seen at low voltage as current is allowed to decay until all Fe^{3+} is consumed. Coulombic efficiency of Fe^{3+} consumption can be calculated as the ratio of useful discharge capacity to total discharge capacity (through both useful discharge and self-discharge). Total discharge capacity is easily determined by weight loss of the iron metal (expressed as mAh theoretical equivalent). Corrosion was ruled out as a significant contributor to metal consumption by soaking an iron block in the electrolyte solution and finding a corrosion rate of roughly 0.8 mA cm^{-2}. Therefore, the inefficiency is ascribed entirely to self-discharge. Self-discharge current was thus estimated to be 7–11 mA cm^{-2} for most discharge runs and severely limits coulombic efficiency and, therefore, utilization at low current density/high voltage.

A practical goal is to maximize energy obtained from the consumable materials. From this standpoint, 25 mA cm^{-2} is the optimum discharge current under constant-current conditions. Energy is constrained by self-discharge at lower current density and cell ASR at higher current density. Separator properties such as thickness, porosity, and permeability impact both limitations, so further separator optimization may lead to improved power. It is anticipated, however, that there is a trade-off between crossover and ohmic resistance when optimizing the membrane, as seen in the Br_2–H_2 redox flow system for which crossover is also a significant limitation at low current density/high voltage.[10] It is also desirable to improve reaction kinetics if they contribute significantly to cell ASR. In fact, the (−) electrode was previously found to be the largest source of voltage loss during discharge for an all-iron cell with high-conductivity electrolyte.[3] The (+) electrode kinetics are not expected to limit cell performance as a current density of an order of magnitude higher is achieved in the iron–hydrogen flow cell with similar electrolyte solution and (+) electrode material.[11] Therefore, further electrode optimization efforts should focus on the (−) electrode.

Practicality and cost

The performance results discussed above can be used to assess the practicality and costs of using the all-iron cell as a primary battery with recharge accomplished by replacing the consumable chemical reactants. Although it is expected that further improvements to performance and efficiency are possible, it is worthwhile to assess the feasibility of this system for the proposed application with the data available. Table 1 shows the design scenario based on the performance at 0.55 V shown in Figure 11 b and a target of providing the end user with 5.4 Wh during a single discharge run, enabling recharging of a mobile phone battery.

Table 1. Design scenario for mobile feature-phone charging.

Component of design	Property		Value
observed performance	energy density	[Wh L^{-1}]	11.5
	power density	[mW cm^{-2}]	18
discharge requirements[a]	energy	[Wh]	5.4
	discharge time	[h]	2
	power	[W]	2.7
size of device	solution volume	[mL]	470
	cell area	[cm^2]	150

[a] Assuming 0.65 Ah phone battery charged at 5 V, through power conditioning circuit that transfers charge from iron battery to phone battery at 60% efficiency.

The cell size and solution volume are reasonable, enabling a small, handheld device. At the 0.5 M $Fe_2(SO_4)_3$ concentration used in the section on discharge behavior, the user would have to mix the consumable chemicals with water to a final volume of 470 mL. Note that decreasing solution concentration below 0.23 M $Fe_2(SO_4)_3$ would result in more than 1 L of water being consumed; this is prohibitive for individuals without easy access to clean water supply. Although it may be desirable to reduce solution concentration to decrease self-discharge, this consideration presents a practical limit. It is worth noting that replacing deionized water with local creek water (Strawberry Creek, Berkeley, CA USA) moderately reduced cell performance in the case of unsupported solutions, but had minimal impact in the case of solutions with supporting electrolyte, as shown in Table 2. The impact of low water quality

Table 2. Impact of untreated creek water, with 0.5 M $Fe_2(SO_4)_3$.

Water supply	Supporting electrolyte		
	none[a]	**1.2 M NaCl**[b]	
	peak power density [mW cm^{-2}]	energy [Wh L^{-1}]	avg. power [mW cm^{-2}]
deionized water	26	12.3	9.3
creek water	19	12.5	9.4

[a] Daramic separator, initial discharge polarization. [b] Paper separator, complete discharge at 0.55 V.

(e.g., dissolved chemicals, heavy metals, suspended particulates, biological contaminants) found throughout the developing world on cell performance should be addressed in the future.

Assuming the power density achieved here is not reduced when scaling up cell size, a cell area of 150 cm^2 (about the size of the human hand) is required to meet the design target. It is expected that the total cell area will be broken down into several smaller cells connected in series to provide the 5 V required by the prevalent USB battery charging standard.[12] Thus, a stack of smaller individual pieces of (+) CPE, separator, and iron foil (−) electrode will be provided for the user to insert into the cell housing. We have found that it is desirable to replace the paper separator after a single complete discharge as the wet paper tends to be damaged upon cell disassembly. In contrast, with careful handling the carbon paper CPE can be reused. At US$80 per m^2,[13] the CPE will cost US$1.20. This is expected to be a significant fraction of the total device cost, which would also include an inexpensive plastic housing, metal electrical contacts, and jack for the phone-charging plug. Further increasing power density to reduce the cell area requirement could, therefore, significantly reduce the total cost of the device to the end user.

Table 3 shows the amount of consumables required per discharge run. The volume of consumables is small and dominated by the salts, which could easily be provided as a single-use packet or tablet about half the size of a deck of cards. The consumables cost for a discharge run is US$0.034 (US$6.45 per kWh), which compares very favorably to kiosk-based mobile-phone charging ($0.25 per charge). Iron sulfate dominates the consumables cost; thus, further cost reductions could be achieved by increasing the Fe^{3+} utilization. At the optimum current and voltage, the utilization is dominated by coulombic inefficiency which could be improved either by increasing the rate of the desired reactions or decreasing the self-discharge rate.

Table 3. Consumables required for each mobile phone charging session.

Component	Weight [g]	Volume [cm^3]	Cost [US$]
$Fe_2(SO_4)_3$	94	30.3	0.023
NaCl	14	6.5	0.001
iron oil	16	2.0	0.008
Office Paper	0.9	1.5	0.002
TOTAL	125	40	0.034

Conclusions

An iron-based redox flow battery was developed and optimized for use as a consumer device for off-grid portable power generation. The constraints of low-cost and non-toxic materials coupled with the concept of the end user recharging the cell manually by replacing consumable materials led to a different materials set and design solution than previous work on the all-iron battery system. $Fe_2(SO_4)_3$ was chosen as the active material for human and environmental health concerns, although this reduces cell performance compared to $FeCl_3$. Extremely inexpensive separator materials including office paper and microporous membrane were found to be suitable. Adding supporting electrolyte to the $Fe_2(SO_4)_3$ solution dramatically increased performance. There is significant scope for future improvements to the cell performance by further optimizing the $Fe_2(SO_4)_3$ and supporting electrolyte concentration, identifying improved CPE materials and structures, and decreasing the impact of self-discharge possibly through separator selection. At the observed power and energy metrics, the cell design is practical in terms of cell size, amount of consumables, volume of water required, and costs, and worth further exploration. Future efforts should include an assessment of environmental and health impact from addition of

NaCl supporting electrolyte, behavior with low-purity water found in the developing world, effect of gravity-fed flow expected for a stand-alone consumer product with no pump, and impact of cell size scaleup.

Experimental Section

Electrolyte solutions were prepared by mixing deionized water with $FeCl_3$ (Sigma–Aldrich), $Fe_2(SO_4)_3$ (Sigma–Aldrich), NaCl (BDH), or Na_2SO_4 (Alfa–Aesar). Low-carbon steel and cast iron sheets were provided by McMaster-Carr. Note both sheets were cleaned with acetone and polished lightly with sand paper before cell assembly to eliminate surface oxidation or machine oil contamination. Porous iron was prepared by sintering a loosely packed bed of pure iron particles at 800 °C in argon. Porous carbon electrode papers were provided by Freudenberg (H2315), SGL (Sigracet 10AA), or Mitsubishi Rayon Co. Ltd (MRC U105).

Solution conductivity and pH value were measured using an Orion Star A325 meter. Viscosity was measured using a Brookfield DVII+ Pro viscometer and CP-42 cone.

Cells were assembled in standard fuel-cell-testing hardware (Fuel Cell Technologies) with 10 cm^2 active area and serpentine flow field on the solution side. The porous carbon electrode and iron electrode were inserted in window-frame-shaped Teflon gaskets, the thickness of which was selected to compress the porous carbon electrode to about 80% of its free-standing thickness. The iron thickness (at least 0.15 mm) was selected to be significantly thicker than necessary so that consumption of iron metal did not limit cell capacity. Electrolyte solution was provided by a peristaltic pump at 60 mL min^{-1} and was recirculated continuously through the cell. Polarization behavior was assessed using 60 mL solution volume to minimize state-of-charge (SOC) variation during the experiment. Experiments where the electrolyte solution was discharged fully used 15 mL solution volume to mimic the expected use case of 1–2 h discharge time. Cells were tested using a VMP-3 (BioLogic) potentiostat with electrochemical impedance spectroscopy capability. Polarization curves were obtained by recording the voltage at the end of 10 s-long current steps, which were found to be long enough to ensure pseudo steady state. Constant-current discharge utilized a voltage limit of 0 V to ensure maximum discharge energy. Constant-voltage discharge utilized a current limit of 2 mA cm^{-2}.

Acknowledgements

This work was funded by the U.S. Department of Energy under contract no. DE-AC02-05CH11231. The authors thank Grace Lau and David Lambelet for assistance with creek water experiments.

Keywords: batteries · electrochemistry · energy conversion · iron

[1] S. Buluswar, Z. Friedman, P. Mehta, S. Mitra, R. Sathre, *50 Breakthroughs: Critical Scientific and Technological Advances Needed for Sustainable Global Development*. LBNL Institute for Globally Transformative Technologies, Berkeley, CA, USA, **2014**.

[2] D. Soto, *IEEE Global Humanitarian Technology Conference* **2014**, 188–191.

[3] L. W. Hruska, R. F. Savinell, *J. Electrochem. Soc.* **1981**, *128*, 18–25.

[4] A. K. Manohar, S. Malkhandi, B. Yang, C. Yang, G. K. S. Prakash, S. R. Narayanan, *J. Electrochem. Soc.* **2012**, *159*, A1209–A1214.

[5] S. Malkhandi, B. Yang, A. K. Manohar, G. K. S. Prakash, S. R. Narayanan, *J. Am. Chem. Soc.* **2013**, *135*, 347–353.

[6] K. L. Hawthorne, T. J. Petek, M. A. Miller, J. S. Wainright, R. F. Savinell, *J. Electrochem. Soc.* **2015**, *162*, A108–A113.

[7] K. L. Hawthorne, J. S. Wainright, R. F. Savinell, *J. Power Sources* **2014**, *269*, 216–224.

[8] K. L. Hawthorne, J. S. Wainright, R. F. Savinell, *J. Electrochem. Soc.* **2014**, *161*, A1662–A1671.

[9] J. A. Mellentine, *Performance Characterization and Cost Assessment of an Iron Hybrid Flow Battery*, University of Iceland and University of Akureyri, MS thesis, **2011**.

[10] M. C. Tucker, K. T. Cho, F. B. Spingler, A. Z. Weber, G. Lin, *J. Power Sources* **2015**, *284*, 212–221.

[11] M. C. Tucker, V. Srinivasan, P. N. Ross, A. Z. Weber, *J. Appl. Electrochem.* **2013**, *43*, 637–644.

[12] USB Battery Charging 1.2 Compliance Plan Revision 1.0, October 12, **2011**, www.USB.org.

[13] K. T. Cho, P. Albertus, V. Battaglia, A. Kojic, V. Srinivasan, A. Z. Weber, *Energy Technol.* **2013**, *1*, 596–608.

Received: June 22, 2015
Revised: October 2, 2015
Published online on November 20, 2015